THE JOURNAL OF PHYSICAL CHEMISTRY B

Article

pubs.acs.org/JPCB

Quantification of Compactness and Local Order in the Ensemble of the Intrinsically Disordered Protein FCP1

Eric B. Gibbs[‡] and Scott A. Showalter*[,‡,§]

[‡]Department of Chemistry, The Pennsylvania State University, University Park, Pennsylvania 16802, United States

[§]Department of Biochemistry and Molecular Biology, The Pennsylvania State University, University Park, Pennsylvania 16802, United States

Supporting Information

ABSTRACT: Intrinsically disordered protein regions (IDRs) partially or completely lack a cooperatively folded structure under native conditions, preventing their equilibrium state from being adequately described by a single structural model. As a direct consequence of their disorder, remarkably few experimental studies have quantified the ensembles IDRs adopt in solution. Here, we conduct unbiased computer simulations of the RAP74 interaction motif from the human phosphatase FCP1 in the unbound state, which provides an ensemble in quantitative agreement with both experimental NMR chemical shift information and small-angle X-ray scattering data. The partially α-helical short linear motif found in the C-terminus of FCP1 has been the subject of extensive biophysical characterization aimed at developing a molecular description for the mechanism of coupled folding and binding and establishing the functional relevance of partial order in the unbound state. The analysis presented here yields a remarkably consistent molecular picture enumerating the diversity of structures present in a "partially formed" helix. Specific interactions, including anticorrelations in backbone dihedral angle fluctuations as well as the transient formation of a helix-stabilizing salt bridge, stabilize the preformed structure in the unbound state. The general consequences of these findings for mechanistic analysis of protein−protein interactions are discussed.

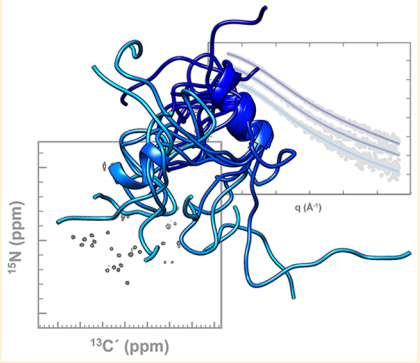

INTRODUCTION

The proteins that carry out transcription, translation, and cellular signaling are highly enriched in intrinsically disordered regions (IDRs) that participate directly in the protein−protein interactions required for these vital functions.[1,2] Given the functional role for IDRs in fundamental biological processes, it is reasonable both to generalize the concept of a protein "domain" to include nonfolding units and to enumerate the ensemble of conformations that IDRs adopt in solution.[3] The tendency of some IDRs to fold into stable conformations upon binding provides additional motivation to evaluate their ensembles in the unbound state because this represents one of two natural thermodynamic end points for the folding-and-binding transition.[4] In the protein folding community, there is a growing awareness of the diversity of structures found in the unfolded state; likewise, it is well-known that IDRs adopt a variety of structures that range from fully disordered to molten globule-like ensembles.[5] Recent progress has advanced quantitative biophysical investigation of IDRs to the point where refining models for their native state is now an attainable goal,[6] but the ensembles adopted by IDRs are generally too heterogeneous for X-ray crystallographic or cryo-electron microscopic characterization to be practical. In contrast, solution methods, including single-molecule fluorescence resonance energy transfer (FRET),[7−10] nuclear magnetic resonance (NMR) spectroscopy,[11−15] and small-angle X-ray scattering (SAXS)[16] have all emerged as powerful tools for the characterization of IDR structure. The combination of NMR and SAXS structural constraints has proven to be especially effective.[17−19]

Our laboratory has conducted an extensive study of the intrinsically disordered recruitment domain from the general transcription factor IIF-associating C-terminal domain (CTD) phosphatase (FCP1). The phosphorylation state of the RNA polymerase II CTD regulates progression through the mRNA biogenesis cycle,[20] where FCP1 phosphatase activity provides an essential component of the regulatory mechanism. Recruitment of FCP1 to RNA polymerase II is mediated by its disordered C-terminal acidic domain.[21−23] Prior to our work, the structure of the FCP1-RAP74 complex was solved to atomic resolution, demonstrating that the bound region of FCP1 forms an amphipathic α-helix in the complex.[22,23] Subsequently, we evaluated the dynamics of the FCP1-RAP74 interaction by both NMR[24] and molecular dynamics (MD),[25,26] demonstrating that FCP1 retains substantial conformational dynamics in the complex. Measurement of the temperature dependence of the FCP1-RAP74 interaction by ITC using a general thermodynamic model in which the large observed

Received: July 11, 2016
Revised: August 15, 2016
Published: August 23, 2016

DOI: 10.1021/acs.jpcb.6b06934
J. Phys. Chem. B 2016, 120, 8960−8969

change in constant-pressure heat capacity is directly fit[27] yielded the conclusion that the thermodynamic driving forces for this binding event are predominantly the same protein−solvent interactions that drive protein folding.[28] These data motivate analysis of the unbound ensemble of FCP1, which we showed qualitatively to be partially α-helical.[29] Predictions made by the Vendruscolo laboratory based on chemical shift information suggest that the same set of residues in the RAP74 binding region of FCP1 is ∼35% helical.[30] Beyond this information, little is known about the molecular details of the ensemble this otherwise well-characterized IDR adopts in solution.

Many excellent reviews have documented recent advances in IDR ensemble determination methods.[13,16,31] Problematically, one theme that emerges from this literature is that IDP ensembles are generally underdetermined by the available experimental constraints, making de novo refinement to unambiguous solutions challenging. Alternatively, with ever increasing computing power available to researchers, it is attractive to consider generating IDP ensembles directly through extensive MD calculations. MD computer simulations are useful because they represent the protein as a conformational ensemble that follows the laws of statistical thermodynamics with the known limitation that the force field chosen for the calculation will influence the outcome.[32] Recently, it has been noted that adding NMR constraints to bias MD trajectories can efficiently yield experimentally informed ensembles.[33−35] Others have observed the utility of combining knowledge-based approaches to ensemble refinement with seed structures generated by MD.[36] Finally, an especially appealing strategy is to collect unbiased MD data for direct hypothesis testing in the context of experimental data. For example, multiple seemingly incompatible structure models of the cardiac protein Troponin 1 were recently shown to be consistent with the distribution of distances sampled by single-molecule FRET and the ensemble of conformers sampled in both MD and Monte Carlo (MC) calculations.[10] This suggests a general strategy in which efficient conformational sampling by MD or MC is coupled to experimental validation of the resulting structure set. Such an approach could represent a general pipeline to generate testable structure−function hypotheses for IDRs.

Here, we conduct unconstrained Monte Carlo computer simulations of the RAP74 binding region from human FCP1 in the unbound state. The resulting conformer sets are tested against experimental NMR chemical shift information and SAXS data. Through this protocol, we were able to evaluate both the overall compactness and the local structure of the ensembles generated. These calculations demonstrate that extensive Monte Carlo sampling using the ABSINTH implicit solvent model, as implemented in the CAMPARI software package,[37,38] quickly leads to ensembles of structures that are mutually consistent with both the SAXS and NMR data sets used for assessment. Additional analysis of the MC-generated structure sets led to enumeration of the atomistic characteristics of the RAP74 binding region of FCP1, yielding molecular insight into the meaning of the qualitative observation of partial helicity in the unbound structure. In general, this suggests an efficient means to better enumerate the properties of short linear motifs (SLiMs;[39] also known as molecular recognition features, or MoRFs[40]), which are recognized to frequently possess nonrandom structure and that are the critical mediators of protein−protein interactions involving intrinsically disordered regions.

MATERIALS AND METHODS

Protein Preparation. FCP1 (residues 930−961) was subcloned from a synthetic gene coding for human FCP1 purchased from Geneart (Invitrogen) into the pET-49b expression vector. Following sequence confirmation, the resulting plasmid was transformed into *Escherichia coli* BL21-(DE3) competent cells. Cell growths for NMR were conducted in M9 media containing $^{15}NH_4Cl$ and u-^{13}C glucose. All growths were maintained at 37 °C until an optical density (OD_{600}) of 0.6 was reached, at which point induction of FCP1-IM gene expression was achieved through the addition of 0.5 mM IPTG. Three hours postinduction, cells were harvested and lysed by sonication, followed by clarification of the soluble fraction through centrifugation at 11500 rpm in a Beckman Coulter Allegra 25R centrifuge using a TA-14-50 rotor. Purification of FCP1-IM from the clarified lysate was accomplished using nickel metal affinity chromatography as previously described.[41] NMR samples were prepared at 1 mM FCP1-IM concentrations in 20 mM sodium phosphate (pH 7.0), 100 mM sodium chloride, 0.02% (w/v) sodium azide, and 10% (v/v) D_2O.

NMR Spectroscopy. Chemical shift assignments of FCP1-IM were confirmed through standard triple resonance ^1H-detected spectroscopy using pulse programs distributed with the Bruker Topspin 3.0 library and ^{13}C-detected spectra collected as previously described.[42] All spectra were collected on a Bruker Avance III spectrometer operating at 500 MHz proton resonance frequency and equipped with a TCI Cryoprobe. Spectra were processed in Topspin prior to analysis in SPARKY (SPARKY 3.113; T. D. Goddard and D. G. Kneller, University of California, San Francisco, CA).

Small-Angle X-ray Scattering. SAXS experiments were performed using FCP1-IM peptides prepared by solid phase synthesis and purified by high-performance liquid chromatography (HPLC, Tufts University Core Facility). FCP1-IM was weighed as lyophilized powder and dissolved into 50 mM MOPS (pH 6.5), 100 mM KCl, 10% glycerol, and 5 mM DTT. Protein concentrations were confirmed by IR spectroscopy using a Direct Detect IR spectrometer (EMD Millipore). SAXS data were collected at the Cornell High Energy Synchrotron Source (CHESS) on the G1 beamline. Incident radiation was produced at 9.963 keV with a flux of $8E^{11}$ photons s^{-1} at 51 mA, providing a q-space range of 0.007−0.7 $Å^{-1}$. Scattering from a silver behenate standard was used for q-axis mapping. Data collection was performed using dual Pilatus 100 K−S detectors. Reduction of the two-dimensional (2D) images to one-dimensional (1D) scattering profiles was performed using BioXtas Raw. Scattering profiles and uncertainties were computed as the average and standard deviation of three exposures with each exposure comprising 20 1 s frames. Solvent blanks were collected immediately before and after each protein sample exposure, and solvent subtraction was performed using equivalent numbers of frames. Data were collected at protein concentrations from 3.6 to 6.8 mg/mL. No signs of aggregation, interparticle effects, or radiation damage were observed. Guinier fitting was performed using the method of nonlinear least-squares in MATLAB (Mathworks) with data fitting restricted to the region satisfying $qR_g < 0.8$ as has been recommended for highly flexible proteins.[43]

DOI: 10.1021/acs.jpcb.6b06934
J. Phys. Chem. B 2016, 120, 8960−8969

ANTON Simulations. Starting conformations of FCP1-IM were generated using the coil library in the TRaDES software package.[44] Two initial conformers were chosen at random, and the unnatural N-terminus was capped in Maestro. These starting protein conformers were then immersed in cubic SPC water boxes with a minimum of 20 Å separating the protein atoms and the box edges; the extra space was provided due to anticipated extreme fluctuations in radius of gyration. Salt in excess of that needed for Ewald cell neutrality was added to a bulk sodium chloride concentration of 50 mM for one simulation and 100 mM for the other. Equilibration of temperature and pressure followed by a 5 ns NPT preproduction run was accomplished locally in Desmond prior to uploading to Anton using a previously reported protocol.[45] All Anton trajectories were run using the 2.4.1 build and the AMBER99SB force field[46] with a 2.0 fs time step and with coordinates saved once every 200 ps. Prior to analysis, solvent molecules were stripped from the snapshots in the VMD software package.[47]

CAMPARI Simulations. Monte Carlo simulations were performed using the CAMPARI software package.[37] All simulations included FCP1-IM in a random starting conformation represented using the OPLSS-AA/L force field and embedded in a cubic box with 250 Å edge lengths. Explicit sodium chloride pairs were included to a final concentration of ∼100 mM with excess sodium to preserve neutrality. The ABSINTH implicit solvation model was used for all trajectories.[38] Replica exchange trajectories were run with 20 replicas at temperatures evenly spanning the range from 230−420 K for 5.1×10^7 steps with the first 1×10^6 steps discarded as equilibration. An additional 20 independent trajectories were run at 310 K for the same number of steps. The move set was composed as follows: rigid body moves, 10% (50%, 10 Å, 20°); side chain moves, 27% (40%, 30°); omega moves, 6.3% (10%, 5°); pucker moves, 0.0%; backbone moves, 56.7% (30%, 10°). Percentages in parentheses correspond to the fraction of fully randomizing moves, while distances and angles represent the maximum displacement and rotation, respectively.

Simulation Analysis. All molecular graphics images were generated using UCSF Chimera.[48] All other analysis was performed in Matlab (MathWorks). Calculation of R_g from the simulated ensembles was performed using CRYSOL, which is a program used to evaluate solution scattering from known structures by fitting to experimental SAXS data.[49] Specifically, CRYSOL was selected from the available software because it has been successfully used to refine conformational ensembles of IDPs.[50] Backbone chemical shifts were calculated from each structure set using the SHIFTS program[51] following the protocol of Li and Brüschweiler.[52] Backbone amide order parameters (S^2) were computed using the isotropic reorientational eigenmode dynamics (iRED) method.[53] Briefly, iRED takes as input a set of structures, such as those generated through MC sampling, and constructs a matrix of the variances and covariances of a set of lattice functions describing the reorientation of selected interaction vectors. For the present analysis, the backbone amide N−H bond orientations, represented by the rank 2 spherical harmonics, provided the lattice functions. The advantage of iRED over related covariance analysis techniques is that it relies on analytical isotropic averaging rather than alignment of structures to a reference frame, which renders the technique well-suited to the analysis of IDPs. If time correlated data are input, such as a set of structures derived from a molecular dynamics trajectory, iRED permits the reconstruction of both correlation times and fluctuation amplitudes. In the present application, where nontime correlated MC data are used as input, we have only used iRED to determine the amplitude of reorientational motion in the calculated structure sets, as reported through S^2.

RESULTS AND DISCUSSION

NMR of FCP1-IM. The C-terminal region of FCP1 (residues 879−961) is intrinsically disordered in solution, but this does not imply that its structure is entirely random. In contrast, the 16 residues constituting the RAP74 binding region (residues 944−960) are partially α-helical in the unbound state.[29] One problem frequently encountered during the course of studying short helical motifs in the context of IDRs is that the preponderance of disordered residues provides a strong signal that masks those from the comparatively short regions of (transient) secondary structure. This was the case for C-terminal FCP1, which had to be truncated for circular dichroism assays to enrich the fraction of signal arising from the α-helical portion.[29] A combination of efficiency in binding studies and computational tractability (see below) has led us to focus on a 32-residue construct that contains the native C-terminal residues 930−961 of the human protein sequence (Figure 1A, top), which we refer to as FCP1-IM (for

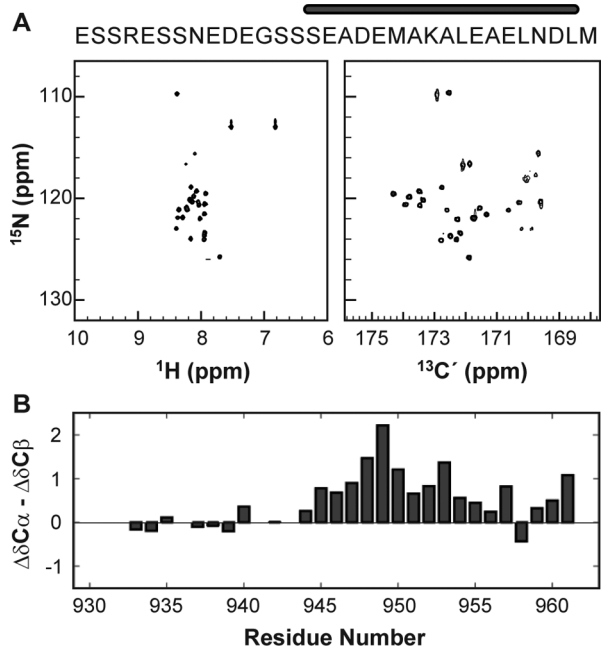

Figure 1. NMR characterization of FCP1-IM reveals chemical shifts consistent with a partially formed α-helix in the RAP74 interaction motif. (A) ^{1}H,^{15}N-HSQC and ^{13}C,^{15}N-CON spectra of FCP1-IM demonstrate excellent chemical shift dispersion. The primary structure of FCP1-IM is displayed above the spectra with the gray bar indicating the RAP74 interaction motif. (B) Secondary $^{13}C^{\alpha}$ and $^{13}C^{\beta}$ chemical shift differences plotted by residue indicate the presence of a well-formed α-helix when a stretch of values >2.0 is encountered.

interaction motif) throughout. In the present study, it was our objective to characterize the solution ensemble of FCP1-IM to generate a molecular understanding of what it means to say that this system is "partially helical" in the unbound state. Representative ^{1}H,^{15}N-HSQC and ^{15}N,^{13}C-CON spectra are shown in Figure 1A, revealing excellent chemical shift dispersion. The structural information encoded in the chemical

DOI: 10.1021/acs.jpcb.6b06934
J. Phys. Chem. B 2016, 120, 8960−8969

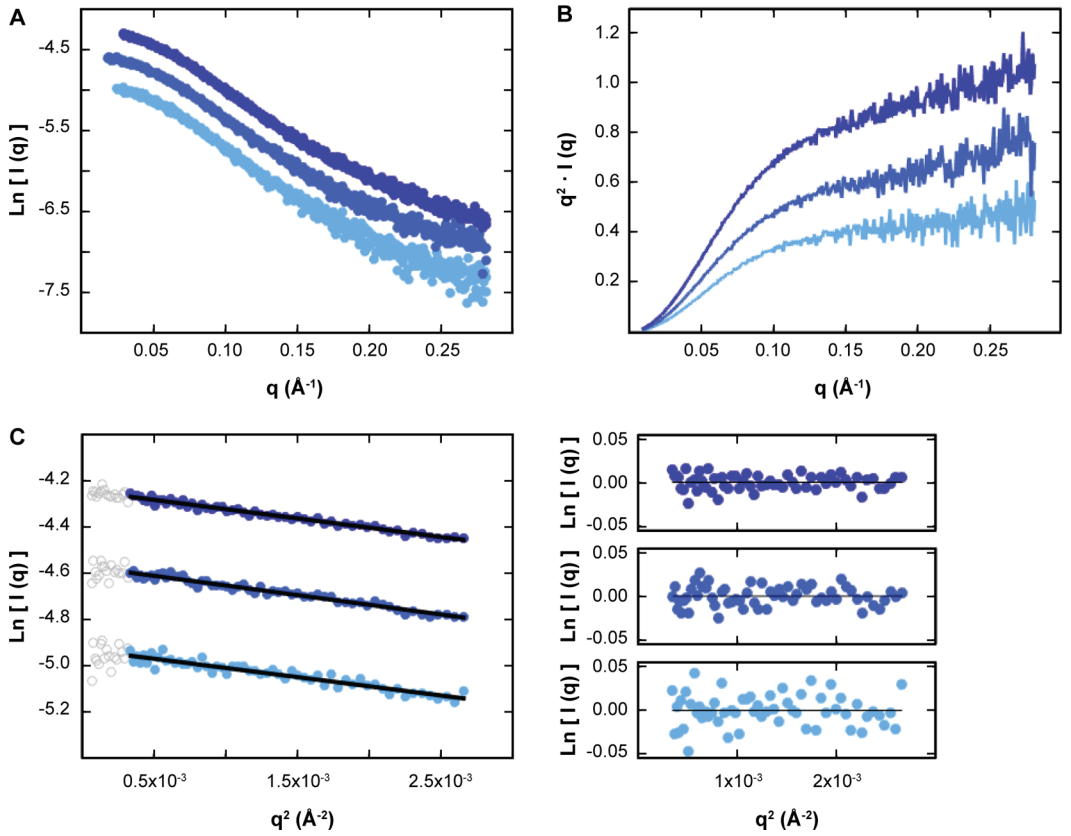

Figure 2. SAXS characterization of FCP1-IM reveals an extended and disordered structure in solution. (A) Raw scattering data for FCP1-IM at concentrations ranging from 3.6−6.8 mg/mL. (B) Kratky plots generated from the data in panel A show a linear increase as a function of q in the high q-region, which is suggestive of a disordered structure in solution. (C) Raw data (blue circles) in the Guinier region and Guinier fits (black lines) for FCP1-IM. Unfitted low q-data points are shown in open gray circles. Data were fit to the Guinier approximation in MATLAB using the method of nonlinear least-squares. Residuals to the fits are displayed on the right.

shift itself has emerged as a key indicator of IDP ensemble properties.[54] For FCP1-IM, acquisition of 3D-HNCACB and 3D-CCCON spectra completed the backbone chemical shift assignment, yielding secondary chemical shift differences that are consistent with partial helical structure in the RAP74 binding region (Figure 1B). The chemical environments and secondary structures of all nonterminal residues are strongly correlated with those found in the longer C-terminal FCP1 construct, for which we have previously reported chemical shift data (Figure S1). These NMR data show that FCP1-IM is a suitable model for the unbound state of the RAP74 binding region of FCP1 in solution.

Small-Angle X-ray Scattering of FCP1-IM. With NMR chemical shifts in hand, we sought an orthogonal technique to constrain the solution ensemble of FCP1-IM. SAXS is complementary to NMR as it provides nanometer scale size and shape information for biomolecules in solution. To eliminate the effects of interparticle interactions, SAXS data for FCP1-IM were collected over a range of protein concentrations, producing scattering curves characteristic of an extended or rod-like molecule (Figure 2A). Likewise, Kratky plots generated from the scattering data displayed a monotonic increase in scattering intensity with increasing scattering angle, consistent with a highly flexible polypeptide (Figure 2B). The low q-region of the scattering curves showed excellent linearity in Guinier plots, strongly suggesting that each sample contained monomeric and noninteracting FCP1-IM particles (Figure 2C). Monodispersity was confirmed by external measurements with dynamic light scattering (Table S1). Scattering intensities at the lowest scattering angles were fit to the Guinier approximation, yielding an average R_g = 15.60 ± 0.12 Å (Figure 2C). For comparison, a chemically denatured 32-mer with sequence $(AAKAA)_6GY$ was shown by SAXS to possess R_g = 14.5 ± 0.6 Å.[55] In contrast, a well-folded (globular) protein with the same number of monomers would display R_g = 6.35 Å. Thus, the global dimensions of FCP1-IM are large relative to the expected value for a folded protein, which suggests that the polypeptide chain samples are an expanded and disordered conformational ensemble in solution.

Molecular Dynamics Simulations of FCP1-IM. An all-atom molecular dynamics simulation of the RAP74-FCP1 complex conducted at a simulation temperature of 298 K showed that FCP1 (residues 944−961) retains key hydrophobic contacts in the context of its complex with RAP74 while experiencing more extensive conformational fluctuations than those that had previously been recognized.[25] Carbon-detected NMR spin relaxation has been used to demonstrate that the C-terminal region of FCP1 is highly dynamic on the ps/ns time scale while free in solution.[24] To our knowledge, no MD trajectories of apo-FCP1 have been reported, which has hindered the description of its solution dynamics at the molecular level. In anticipation that extensive conformational sampling would be required to accurately represent the solution ensemble of FCP1-IM, we turned to computation on the purpose-built Anton molecular dynamics machine to achieve multiple microseconds of production MD.[56] As summarized in

DOI: 10.1021/acs.jpcb.6b06934
J. Phys. Chem. B 2016, 120, 8960−8969

Figures S2 and S3, the two calculated trajectories each sampled α-helical conformations in the correct location, but neither simulation achieved the correct balance between helical and extended conformations. Further, the second simulation collapsed into a metastable and highly compact state ~1.5 μs into the trajectory from which it never escaped (Figure S3). Overall, the Anton trajectories were found to capture the qualitative behavior of FCP1-IM, but quantitative comparison with experiments was not successful. Concurrent with our study, Best and co-workers developed force field modifications that were designed to overcome known imbalances in the strength of interactions between solute proteins and solvent waters in the Amber family of force fields.[57] One recent application of the modified force field demonstrates that it successfully relieves the tendency of IDRs to adopt overly compact conformations in MD simulations,[58] suggesting a future path to successful dynamics computations for FCP1 and related disordered proteins.

CAMPARI Simulations of FCP1-IM. The objective of this work was to establish a molecular ensemble representation of FCP1-IM that is consistent with averaged experimental properties, which suggests that the rich dynamic information encoded in an MD trajectory is less central to the task than efficient sampling of conformational space. Recently, the Pappu laboratory established the efficiency of Monte Carlo sampling of IDR conformational space using an all-atom representation of the protein and ions solvated in the ABSINTH implicit water model.[37,38] As an initial test of the feasibility of calculating MC trajectories for FCP1-IM, we conducted a thermal replica exchange MC (REMC) simulation sampling 20 temperatures spanning 230−420 K (see Materials and Methods). The average R_g computed directly from the snapshots displayed a sigmoidal increase as a function of temperature with the 300 K replica occupying the inflection point (Figure S4). At all temperatures in the transition region, both R_g and the asphericity of the conformers experienced robust fluctuations (Figure S5) consistent with previous recommendations for identifying well-sampled trajectories.[59] Significantly, a strong preference for the α-helical conformation was observed for residues 948−956 at low temperature, which melted out monotonically as a function of temperature and was completely lost above 340 K (Figure S6). With this information from the REMC simulation in hand, we next conducted an extensive set of single-temperature MC calculations at 290, 300, 310, and 320 K. The best agreement with experimental NMR and SAXS data was observed in the 310 K simulations, which are therefore discussed here in more detail.

Twenty independent MC simulations of FCP1-IM were conducted at 310 K. Each trajectory was independently analyzed prior to pooling the generated snapshots, revealing substantial variations in the average helicity of the RAP74 binding region (Figure S6) accompanied by excellent sampling of the R_g and asphericity (Figure S7). Pooling the snapshots from the full set of simulations yields an R_g distribution that is maximal at ~12 Å with substantial population fractions persisting to >20 Å (Figure 3A). Significantly, all bins in the histogram except those that represent the most extended chains contain both conformers that are enriched in α-helical character and conformers that are better described as coil-like for all residues. Computation of the hydrated R_g in CRYSOL for the pool of conformers from the 310 K trajectories yields a median R_g = 15.79 Å, which is in excellent agreement with the experimental value of 15.60 ± 0.12 Å from SAXS (Table S1).

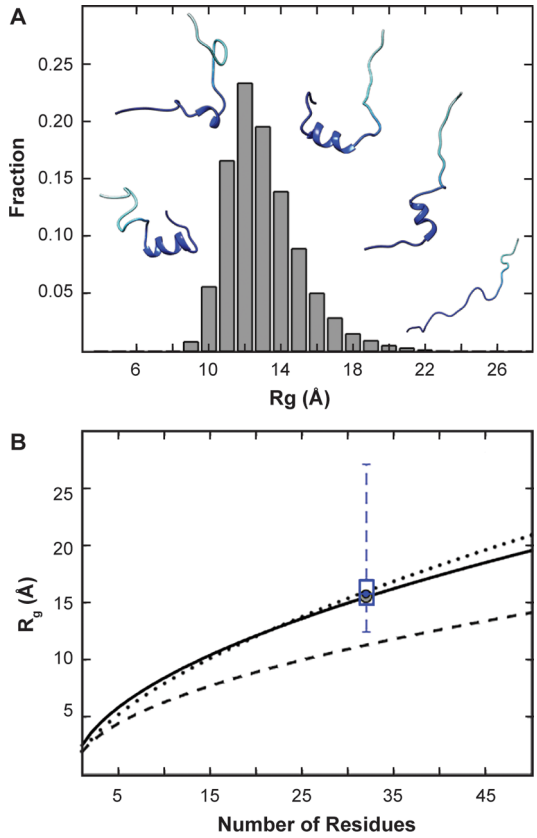

Figure 3. Compactness of FCP1-IM in solution is well reproduced by the conformers generated through MC sampling. (A) Histogram of the R_g calculated for each snapshot based on the atomic coordinates. Five representative conformers from the 10, 12, 14, 16, and 20 Å bins are displayed as blue ribbon diagrams. (B) The median radius of gyration (R_g) from conformations sampled in the set of 20 MC simulations computed at 310 K (blue marker) is consistent with experimental results (gray dot). The box plot (blue) represents the median, quartiles, and range of R_g from the simulations. Reference R_g values computed for a protein in theta solvent (dashed line), good solvent (black line), and an experimentally determined curve for IDPs (dotted line)[16] are provided, showing that FCP1-IM behaves as a polypeptide in a good solvent under the experimental conditions.

To place the measured R_g in context, Figure 3B also displays the expectation value for a statistical coil in a theta solvent (dashed line) or good solvent (solid line) as well as the expectation value based on a recent analysis of available IDP data sets[16,60] (dotted line).

In addition to modeling the compactness of the FCP1-IM ensemble well, the pool of MC-derived conformers also accurately reproduces the location and probability of α-helical conformation. The average helicity identified by DSSP for residues 948−956 is 41.8% (Figure 4A), which is in good agreement with previous predictions based on NMR chemical shifts[30] or native-based simulations.[26] Carbon chemical shifts were back calculated from the conformer set and used to generate the difference in deviation from random coil chemical shifts for Cα and Cβ ($\Delta\delta C\alpha - \Delta\delta C\beta$), which is a well-accepted metric for the extent of helical structure encoded in NMR chemical shift information.[61] The overall agreement between the MC predicted values and measured NMR chemical shift differences was excellent (Figure 4B). Most encouragingly, the residues that display the strongest tendency to adopt α-helical structure in the MC simulations matches well

DOI: 10.1021/acs.jpcb.6b06934
J. Phys. Chem. B 2016, 120, 8960−8969

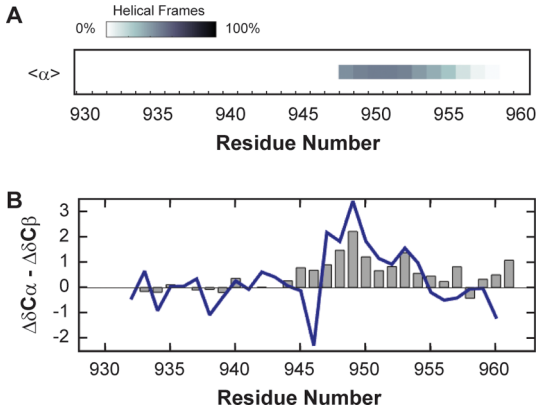

Figure 4. Local tendency for amino acid residues in FCP1-IM to form an α-helix in solution is reproduced well by conformers generated through MC sampling. (A) Average helical frames sampled in the set of 20 MC simulations computed at 310 K are represented by residue in greyscale (see legend above panel), indicating a tendency toward helical structure in residues 947−956. (B) Predicted secondary chemical shift differences computed from the pooled structures generated by MC sampling at 310 K (blue line) are highly consistent with the experimental values (gray bars).

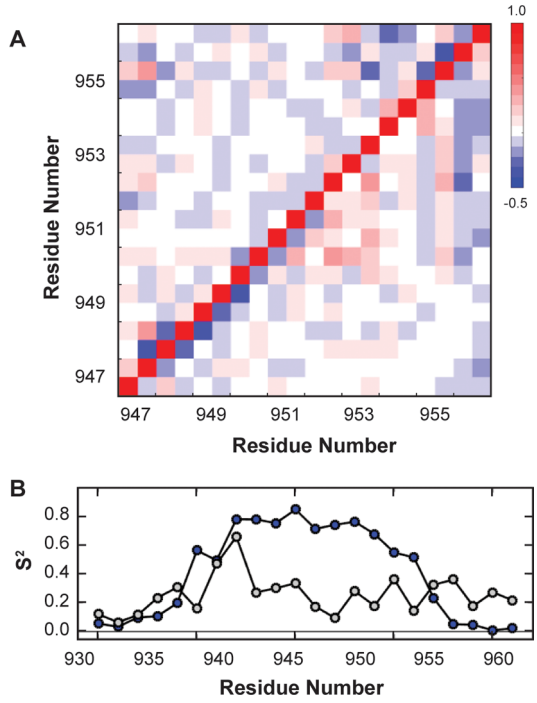

Figure 5. Presence of negative φ_i/ψ_{i-1} correlations in FCP1-IM promotes internal order in residues that adopt an α-helix conformation. (A) The correlation coefficients between the backbone torsion angles φ and ψ in the RAP74 interaction motif are generally weak except for the crankshaft anticorrelation observed when the protein adopts an α-helix conformation. Correlations above the diagonal represent the MC simulation with the lowest fraction of frames sampling α-helix, while those below the diagonal are calculated from the MC simulation with the highest fraction of helical frames. The color bar to the right demonstrates the gradient between $r = -0.5$ (blue) and $r = 1.0$ (red) with $r = 0$ set to white in the color map. (B) The order parameter S^2 generated using the iRED method is plotted as a function of residue number for the MC simulation with the lowest fraction of frames sampling α-helix (gray circles) and the MC simulation with the highest fraction of helical frames (blue circles).

to the set of residues identified by NMR chemical shift and urea denaturation as being partially helical in solution.

The conformations of FCP1-IM sampled in the traditional and REMC simulations possess structural features that are consistent with the expected behavior of a helix-forming peptide in solution. The defining characteristic of loop-closing hydrogen bonds formed between the backbone carbonyl oxygen and amide nitrogen of residues i and $i + 4$, respectively, has already been documented in these ensembles through the DSSP calculations summarized in Figure 4. An additional well-documented feature of α-helical structure is the "crankshaft" anticorrelation between the backbone torsion angles φ_i and ψ_{i-1}, which facilitates retention of the overall α-helical structure in the presence of thermally driven fluctuations in the peptide plane orientation.[62,63] It has been shown that random sampling of Ramachandran space is capable of producing physically unrealistic conformers that possess α-helical hydrogen bonds but which lack the necessary crankshaft anticorrelations.[64] In contrast, the MC-generated conformers display the expected backbone conformational behavior for a peptide in solution; residues 947−952 show robust anticorrelations consistent with crankshaft motion in the simulations that feature strong helical character which are absent in the simulations with lower α-helix content (Figure 5A). Strong crankshaft anticorrelations promote order in the peptide backbone, as demonstrated in model peptide studies where greater generalized order parameters (S^2) corresponding to internal dynamics of the backbone amide bond correlated with stronger crankshaft correlations.[64] Consistent with this observation, the internal order represented by S^2 is greatest in the MC simulations that favor α-helix formation and weakest in those lacking significant helical character (Figure 5B). Overall, the molecular features of the FCP1-IM backbone are consistent with the known physical/chemical properties of helix-forming peptides.

Having established that the backbone of FCP1-IM sample conformational states that are both physically reasonable and consistent with experimental measurements, we next sought to establish whether our MC results might yield insight into the binding mechanism that forms the FCP1-RAP74 complex. FCP1-IM is a strong polyampholyte, possessing a 0.41 fraction of charged residues and a −0.28 net charge per residue, which is consistent with the observation of an expanded solution ensemble.[65] Given this information and the basic character of the RAP74 surface, it is surprising that the FCP1-RAP74 complex contains only one favorable salt bridge formed in trans (D947 to K471, Figure 6A).[22] Although the contribution of salt bridges to fold stability has long been questioned,[66] the mutation D947A eliminates the FCP1-RAP74 interaction in pulldown assays, suggesting this interaction is as critical to binding as the deep burial of hydrophobic residues into the binding cleft.[22] FCP1-IM possesses two positively charged residues (R933 and K951), and therefore we analyzed the MC ensembles to determine whether salt bridges are formed to a substantial population. Strikingly, the only salt bridge formed in >2% of the conformers was found between D947 and K951 (Figures 6A and B). There is a strong correlation between the presence of this salt bridge and assignment of the intervening residue A950 to α-helical conformation by DSSP (Figure 6B), suggesting that this interaction contributes to the stability of α-helical structure in the apo-state. This observation is consistent with previous native-based simulations that show that the transition state for FCP1 binding by RAP74 is characterized by the formation of native contacts in the N-terminal region of the

DOI: 10.1021/acs.jpcb.6b06934
J. Phys. Chem. B 2016, 120, 8960−8969

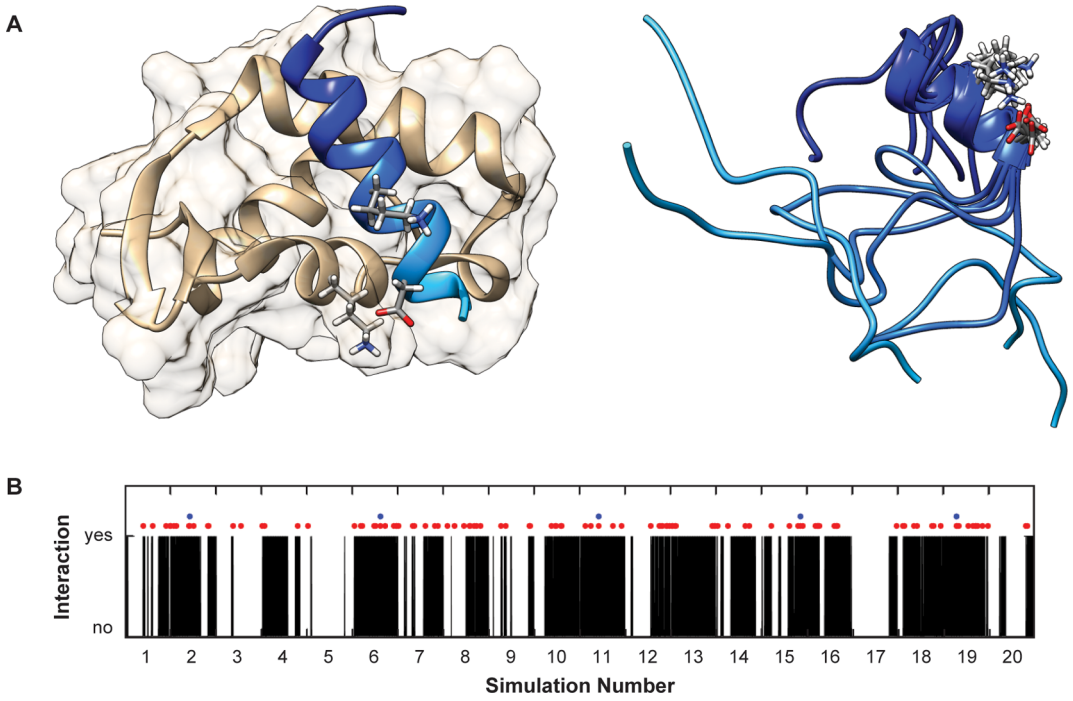

Figure 6. Formation of a D947/K951 salt bridge promotes the formation of an α-helix in the unbound state of FCP1-IM but is not necessary in the FCP1-RAP74 complex, whereas D947 instead forms a salt bridge with the RAP74 residue K471. (A) The cocrystal structure of an FCP1 peptide bound to RAP74 (left) reveals that D947 is positioned to form a salt bridge with K471, but not with K951. The three key residues are displayed in CPK, while the remainder of FCP1 and RAP74 are displayed as blue and tan ribbon diagrams, respectively. On the right, five representative structures in which an α-helix and also the D947/K951 salt bridge are formed in apo-FCP1-IM simulations are displayed as blue ribbon diagrams with D947 and K951 represented in CPK mode. (B) Assignment of A950 to α-helix by DSSP is plotted as a function of frame across each of the 20 MC simulations computed at 310 K (black bars). Adoption of the α-helix by this residue that is found between K947 and K951 correlates strongly with the frames in which the side-chain centers of charge from these two residues are $\leq$5 Å from one another (red circles). The five frames represented in panel A on the right-hand side are indicated by blue circles, showing that these highly similar conformers are sampled in multiple independent MC simulations.

FCP1 α-helix and the formation of interface-spanning contacts involving the same residues.[26] In contrast, FCP1-K951A is fully competent to pull down RAP74,[22] suggesting that this salt bridge does not stabilize the final complex. Recent work with model peptides has shown that salt bridges placed to support helical geometry can speed up α-helix folding kinetics, thus contributing favorably to folding or complex formation even when the salt bridge itself does not contribute to the stability of the folded state.[67] Inspection of the FCP1-RAP74 cocrystal structure (Figure 6A, left) and five representative conformers chosen from independent trajectories but possessing the D947/K951 salt bridge (Figure 6A, right) suggests a speculative mechanism in which the intramolecular salt bridge favors conformations near the binding transition state prior to hand-off of D947 to form a stabilizing salt bridge with K471 of RAP74 in the final complex.

CONCLUSIONS

Intrinsically disordered proteins have emerged as critical components of the proteome, in which they appear to be ideally suited to perform cellular functions that necessitate reversible protein−protein interaction. Significantly, as more is learned about the physical/chemical properties of disordered proteins, it has become increasingly clear that they possess more characteristics in common with their cooperatively folded counterparts than previously thought; they simply fail to fold in the unbound state. Even so, rigorous determination of disordered protein conformational ensembles remains challenging, largely because the available structural constraints (e.g., smFRET, NMR, or SAXS) underdetermine the computed ensembles. Here, we have taken the approach of calculating ensembles through molecular dynamics and Monte Carlo methods, unbiased by the input of experimental data, for the well-studied RAP74 interaction motif of the phosphatase FCP1. Analysis of MC ensembles in particular reveals a set of structures strongly consistent with both the global structural features measured by SAXS and the local structural preferences enumerated by NMR. Significantly, analysis of the ensemble vetted by these comparisons yields deep insight into the nature of the "partially helical" structure previously attributed to the FCP1 interaction motif in solution and generates predictive insights into the nature of binding between FCP1 and its partner RAP74. The data presented here lead directly to a mechanistic understanding of preformed structure in the unbound state of FCP1 and generate testable thermodynamic and kinetic predictions. While substantial effort has been put into determining the thermodynamic consequences for coupling disorder-to-order transitions with binding, there has been a recent push toward more thoroughly characterizing the impact of intrinsic protein disorder on the kinetics of binding events and the consequences disorder has for mechanism and biological function.[68] In this context, it is clear that modeling and structure refinement of disordered proteins have matured to the point where long-standing gaps in knowledge of the kinetic mechanism associated with transient protein binding

DOI: 10.1021/acs.jpcb.6b06934
J. Phys. Chem. B 2016, 120, 8960−8969

and the source of the apparent selective preference for disorder in many of these events can be quantitatively addressed.

■ ASSOCIATED CONTENT

Supporting Information

The Supporting Information is available free of charge on the ACS Publications website at DOI: 10.1021/acs.jpcb.6b06934.

Table of SAXS acquisition and analysis parameters, additional MD analysis, and additional CAMPARI analysis (PDF)

■ AUTHOR INFORMATION

Corresponding Author

*E-mail: sas76@psu.edu, Phone: 1-814-865-2138.

Notes

The authors declare no competing financial interest.

■ ACKNOWLEDGMENTS

We are grateful to Dr. Lois Pollack and Joshua Tokuda for their assistance with acquiring and interpreting the SAXS data. This work was supported by US National Science Foundation CAREER Grant MCB-0953918 and MCB-1515974 to S.A.S. and an Arthur P. Sloan MPHD fellowship to E.B.G. The Anton machine at the National Resource for Biomedical Supercomputing/Pittsburgh Supercomputing Center was generously made available by D.E. Shaw Research. Anton computer time was provided by the National Resource for Biomedical Supercomputing and the Pittsburgh Supercomputing Center through US National Institutes of Health Grant RC2-GM093307. This work is based upon research conducted at the Cornell High Energy Synchrotron Source (CHESS), which is supported by the National Science Foundation and the National Institutes of Health/National Institute of General Medical Sciences under NSF awards DMR-1332208 and DMR-0936384, using the Macromolecular Diffraction at CHESS (MacCHESS) facility, which is supported by award GM-103485 from the National Institute of General Medical Sciences, National Institutes of Health.

■ REFERENCES

(1) Fuxreiter, M.; Tompa, P.; Simon, I.; Uversky, V. N.; Hansen, J. C.; Asturias, F. J. Malleable Machines Take Shape in Eukaryotic Transcriptional Regulation. *Nat. Chem. Biol.* **2008**, *4*, 728−737.

(2) Tantos, A.; Han, K. H.; Tompa, P. Intrinsic Disorder in Cell Signaling and Gene Transcription. *Mol. Cell. Endocrinol.* **2012**, *348*, 457−465.

(3) Das, R. K.; Ruff, K. M.; Pappu, R. V. Relating Sequence Encoded Information to Form and Function of Intrinsically Disordered Proteins. *Curr. Opin. Struct. Biol.* **2015**, *32*, 102−112.

(4) Csermely, P.; Palotai, R.; Nussinov, R. Induced Fit, Conformational Selection and Independent Dynamic Segments: An Extended View of Binding Events. *Trends Biochem. Sci.* **2010**, *35*, 539−546.

(5) van der Lee, R.; Buljan, M.; Lang, B.; Weatheritt, R. J.; Daughdrill, G. W.; Dunker, A. K.; Fuxreiter, M.; Gough, J.; Gsponer, J.; Jones, D. T.; et al. Classification of Intrinsically Disordered Regions and Proteins. *Chem. Rev.* **2014**, *114*, 6589−6631.

(6) Gibbs, E. B.; Showalter, S. A. Quantitative Biophysical Characterization of Intrinsically Disordered Proteins. *Biochemistry* **2015**, *54*, 1314−1326.

(7) Mukhopadhyay, S.; Krishnan, R.; Lemke, E. A.; Lindquist, S.; Deniz, A. A. A Natively Unfolded Yeast Prion Monomer Adopts an Ensemble of Collapsed and Rapidly Fluctuating Structures. *Proc. Natl. Acad. Sci. U. S. A.* **2007**, *104*, 2649−2654.

(8) Ferreon, A. C.; Gambin, Y.; Lemke, E. A.; Deniz, A. A. Interplay of Alpha-Synuclein Binding and Conformational Switching Probed by Single-Molecule Fluorescence. *Proc. Natl. Acad. Sci. U. S. A.* **2009**, *106*, 5645−5650.

(9) Ducas, V. C.; Rhoades, E. Investigation of Intramolecular Dynamics and Conformations of Alpha-, Beta- and Gamma-Synuclein. *PLoS One* **2014**, *9*, e86983.

(10) Metskas, L. A.; Rhoades, E. Conformation and Dynamics of the Troponin I C-Terminal Domain: Combining Single-Molecule and Computational Approaches for a Disordered Protein Region. *J. Am. Chem. Soc.* **2015**, *137*, 11962−11969.

(11) Dyson, H. J.; Wright, P. E. Unfolded Proteins and Protein Folding Studied by Nmr. *Chem. Rev.* **2004**, *104*, 3607−3622.

(12) Shi, Z. S.; Chen, K.; Liu, Z. G.; Kallenbach, N. R. Conformation of the Backbone in Unfolded Proteins. *Chem. Rev.* **2006**, *106*, 1877−1897.

(13) Mittag, T.; Forman-Kay, J. D. Atomic-Level Characterization of Disordered Protein Ensembles. *Curr. Opin. Struct. Biol.* **2007**, *17*, 3−14.

(14) Jensen, M. R.; Ruigrok, R. W.; Blackledge, M. Describing Intrinsically Disordered Proteins at Atomic Resolution by Nmr. *Curr. Opin. Struct. Biol.* **2013**, *23*, 426−435.

(15) Jensen, M. R.; Zweckstetter, M.; Huang, J. R.; Blackledge, M. Exploring Free-Energy Landscapes of Intrinsically Disordered Proteins at Atomic Resolution Using Nmr Spectroscopy. *Chem. Rev.* **2014**, *114*, 6632−6660.

(16) Bernado, P.; Svergun, D. I. Structural Analysis of Intrinsically Disordered Proteins by Small-Angle X-Ray Scattering. *Mol. BioSyst.* **2012**, *8*, 151−167.

(17) Sibille, N.; Bernado, P. Structural Characterization of Intrinsically Disordered Proteins by the Combined Use of Nmr and Saxs. *Biochem. Soc. Trans.* **2012**, *40*, 955−962.

(18) Schwalbe, M.; Ozenne, V.; Bibow, S.; Jaremko, M.; Jaremko, L.; Gajda, M.; Jensen, M. R.; Biernat, J.; Becker, S.; Mandelkow, E.; et al. Predictive Atomic Resolution Descriptions of Intrinsically Disordered Htau40 and Alpha-Synuclein in Solution from Nmr and Small Angle Scattering. *Structure* **2014**, *22*, 238−249.

(19) Hennig, J.; Sattler, M. The Dynamic Duo: Combining NMR and Small Angle Scattering in Structural Biology. *Protein Sci.* **2014**, *23*, 669−682.

(20) Meinhart, A.; Kamenski, T.; Hoeppner, S.; Baumli, S.; Cramer, P. A Structural Perspective of Ctd Function. *Genes Dev.* **2005**, *19*, 1401−1415.

(21) Archambault, J.; Pan, G. H.; Dahmus, G. K.; Cartier, M.; Marshall, N.; Zhang, S.; Dahmus, M. E.; Greenblatt, J. Fcp1, the Rap74-Interacting Subunit of a Human Protein Phosphatase That Dephosphorylates the Carboxyl-Terminal Domain of Rna Polymerase Iio. *J. Biol. Chem.* **1998**, *273*, 27593−27601.

(22) Kamada, K.; Roeder, R. G.; Burley, S. K. Molecular Mechanism of Recruitment of Tfiif-Associating Rna Polymerase C-Terminal Domain Phosphatase (Fcp1) by Transcription Factor Iif. *Proc. Natl. Acad. Sci. U. S. A.* **2003**, *100*, 2296−2299.

(23) Nguyen, B. D.; Abbott, K. L.; Potempa, K.; Kobor, M. S.; Archambault, J.; Greenblatt, J.; Legault, P.; Omichinski, J. G. Nmr Structure of a Complex Containing the Tfiif Subunit Rap74 and the Rna Polymerase Ii Carboxyl-Terminal Domain Phosphatase Fcp1. *Proc. Natl. Acad. Sci. U. S. A.* **2003**, *100*, 5688−5693.

(24) Lawrence, C. W.; Showalter, S. A. Carbon-Detected N-15 NMR Spin Relaxation of an Intrinsically Disordered Protein: Fcp1 Dynamics Unbound and in Complex with Rap74. *J. Phys. Chem. Lett.* **2012**, *3*, 1409−1413.

(25) Wostenberg, C.; Kumar, S.; Noid, W. G.; Showalter, S. A. Atomistic Simulations Reveal Structural Disorder in the Rap74-Fcp1 Complex. *J. Phys. Chem. B* **2011**, *115*, 13731−13739.

(26) Kumar, S.; Showalter, S. A.; Noid, W. G. Native-Based Simulations of the Binding Interaction between Rap74 and the Disordered Fcp1 Peptide. *J. Phys. Chem. B* **2013**, *117*, 3074−3085.

(27) Sahu, D.; Bastidas, M.; Lawrence, C. W.; Noid, W. G.; Showalter, S. A. Assessing Coupled Protein Folding and Binding

DOI: 10.1021/acs.jpcb.6b06934
J. Phys. Chem. B 2016, 120, 8960−8969

through Temperature-Dependent Isothermal Titration Calorimetry. *Methods Enzymol.* **2016**, *567*, 23−45.
(28) Lawrence, C. W.; Kumar, S.; Noid, W. G.; Showalter, S. A. Role of Ordered Proteins in the Folding-Upon-Binding of Intrinsically Disordered Proteins. *J. Phys. Chem. Lett.* **2014**, *5*, 833−838.
(29) Lawrence, C. W.; Bonny, A.; Showalter, S. A. The Disordered C-Terminus of the Rna Polymerase Ii Phosphatase Fcp1 Is Partially Helical in the Unbound State. *Biochem. Biophys. Res. Commun.* **2011**, *410*, 461−465.
(30) Camilloni, C.; De Simone, A.; Vranken, W. F.; Vendruscolo, M. Determination of Secondary Structure Populations in Disordered States of Proteins Using Nuclear Magnetic Resonance Chemical Shifts. *Biochemistry* **2012**, *51*, 2224−2231.
(31) Salmon, L.; Blackledge, M. Investigating Protein Conformational Energy Landscapes and Atomic Resolution Dynamics from Nmr Dipolar Couplings: A Review. *Rep. Prog. Phys.* **2015**, *78*, 126601.
(32) Guerry, P.; Mollica, L.; Blackledge, M. Mapping Protein Conformational Energy Landscapes Using Nmr and Molecular Simulation. *ChemPhysChem* **2013**, *14*, 3046−3058.
(33) Dedmon, M. M.; Lindorff-Larsen, K.; Christodoulou, J.; Vendruscolo, M.; Dobson, C. M. Mapping Long-Range Interactions in Alpha-Synuclein Using Spin-Label Nmr and Ensemble Molecular Dynamics Simulations. *J. Am. Chem. Soc.* **2005**, *127*, 476−477.
(34) Richter, B.; Gsponer, J.; Varnai, P.; Salvatella, X.; Vendruscolo, M. The Mumo (Minimal under-Restraining Minimal over-Restraining) Method for the Determination of Native State Ensembles of Proteins. *J. Biomol. NMR* **2007**, *37*, 117−135.
(35) Lindorff-Larsen, K.; Kristjansdottir, S.; Teilum, K.; Fieber, W.; Dobson, C. M.; Poulsen, F. M.; Vendruscolo, M. Determination of an Ensemble of Structures Representing the Denatured State of the Bovine Acyl-Coenzyme a Binding Protein. *J. Am. Chem. Soc.* **2004**, *126*, 3291−3299.
(36) Ball, K. A.; Phillips, A. H.; Wemmer, D. E.; Head-Gordon, T. Differences in Beta-Strand Populations of Monomeric Abeta40 and Abeta42. *Biophys. J.* **2013**, *104*, 2714−2724.
(37) Vitalis, A.; Pappu, R. V. Methods for Monte Carlo Simulations of Biomacromolecules. *Annu. Rep. Comput. Chem.* **2009**, *5*, 49−76.
(38) Vitalis, A.; Pappu, R. V. Absinth: A New Continuum Solvation Model for Simulations of Polypeptides in Aqueous Solutions. *J. Comput. Chem.* **2009**, *30*, 673−699.
(39) Van Roey, K.; Uyar, B.; Weatheritt, R. J.; Dinkel, H.; Seiler, M.; Budd, A.; Gibson, T. J.; Davey, N. E. Short Linear Motifs: Ubiquitous and Functionally Diverse Protein Interaction Modules Directing Cell Regulation. *Chem. Rev.* **2014**, *114*, 6733−6778.
(40) Mohan, A.; Oldfield, C. J.; Radivojac, P.; Vacic, V.; Cortese, M. S.; Dunker, A. K.; Uversky, V. N. Analysis of Molecular Recognition Features (Morfs). *J. Mol. Biol.* **2006**, *362*, 1043−1059.
(41) Showalter, S. A. Nmr Assignment of the Intrinsically Disordered C-Terminal Region of Homo Sapiens Fcp1 in the Unbound State. *Biomol. NMR Assignments* **2009**, *3*, 179−181.
(42) Bastidas, M.; Gibbs, E. B.; Sahu, D.; Showalter, S. A. A Primer for Carbon-Detected Nmr Applications to Intrinsically Disordered Proteins in Solution. *Concepts Magn. Reson., Part A* **2015**, *44*, 54−66.
(43) Receveur-Brechot, V.; Durand, D. How Random Are Intrinsically Disordered Proteins? A Small Angle Scattering Perspective. *Curr. Protein Pept. Sci.* **2012**, *13*, 55−75.
(44) Feldman, H. J.; Hogue, C. W. A Fast Method to Sample Real Protein Conformational Space. *Proteins: Struct., Funct., Genet.* **2000**, *39*, 112−131.
(45) Bastidas, M.; Showalter, S. A. Thermodynamic and Structural Determinants of Differential Pdx1 Binding to Elements from the Insulin and Iapp Promoters. *J. Mol. Biol.* **2013**, *425*, 3360−3377.
(46) Hornak, V.; Abel, R.; Okur, A.; Strockbine, B.; Roitberg, A.; Simmerling, C. Comparison of Multiple Amber Force Fields and Development of Improved Protein Backbone Parameters. *Proteins: Struct., Funct., Genet.* **2006**, *65*, 712−725.
(47) Humphrey, W.; Dalke, A.; Schulten, K. Vmd: Visual Molecular Dynamics. *J. Mol. Graphics* **1996**, *14*, 33−38 and 27−38..
(48) Pettersen, E. F.; Goddard, T. D.; Huang, C. C.; Couch, G. S.; Greenblatt, D. M.; Meng, E. C.; Ferrin, T. E. Ucsf Chimera–a Visualization System for Exploratory Research and Analysis. *J. Comput. Chem.* **2004**, *25*, 1605−1612.
(49) Svergun, D.; Barberato, C.; Koch, M. H. J. Crysol - a Program to Evaluate X-Ray Solution Scattering of Biological Macromolecules from Atomic Coordinates. *J. Appl. Crystallogr.* **1995**, *28*, 768−773.
(50) Krzeminski, M.; Marsh, J. A.; Neale, C.; Choy, W. Y.; Forman-Kay, J. D. Characterization of Disordered Proteins with Ensemble. *Bioinformatics* **2013**, *29*, 398−399.
(51) Xu, X. P.; Case, D. A. Automated Prediction of N-15, C-13(Alpha), C-13(Beta) and C-13 ′ Chemical Shifts in Proteins Using a Density Functional Database. *J. Biomol. NMR* **2001**, *21*, 321−333.
(52) Li, D. W.; Brüschweiler, R. Certification of Molecular Dynamics Trajectories with Nmr Chemical Shifts. *J. Phys. Chem. Lett.* **2010**, *1*, 246−248.
(53) Prompers, J. J.; Brüschweiler, R. General Framework for Studying the Dynamics of Folded and Nonfolded Proteins by Nmr Relaxation Spectroscopy and Md Simulation. *J. Am. Chem. Soc.* **2002**, *124*, 4522−4534.
(54) Jensen, M. R.; Salmon, L.; Nodet, G.; Blackledge, M. Defining Conformational Ensembles of Intrinsically Disordered and Partially Folded Proteins Directly from Chemical Shifts. *J. Am. Chem. Soc.* **2010**, *132*, 1270−1272.
(55) Kohn, J. E.; Millett, I. S.; Jacob, J.; Zagrovic, B.; Dillon, T. M.; Cingel, N.; Dothager, R. S.; Seifert, S.; Thiyagarajan, P.; Sosnick, T. R.; et al. Random-Coil Behavior and the Dimensions of Chemically Unfolded Proteins. *Proc. Natl. Acad. Sci. U. S. A.* **2004**, *101*, 12491−12496.
(56) Shaw, D. E.; Deneroff, M. M.; Dror, R. O.; Kuskin, J. S.; Larson, R. H.; Salmon, J. K.; Young, C.; Batson, B.; Bowers, K. J.; Chao, J. C.; et al. Anton, a Special-Purpose Machine for Molecular Dynamics Simulation. *Commun. ACM* **2008**, *51*, 91−97.
(57) Best, R. B.; Zheng, W.; Mittal, J. Balanced Protein-Water Interactions Improve Properties of Disordered Proteins and Non-Specific Protein Association. *J. Chem. Theory Comput.* **2014**, *10*, 5113−5124.
(58) Rauscher, S.; Gapsys, V.; Gajda, M. J.; Zweckstetter, M.; de Groot, B. L.; Grubmuller, H. Structural Ensembles of Intrinsically Disordered Proteins Depend Strongly on Force Field: A Comparison to Experiment. *J. Chem. Theory Comput.* **2015**, *11*, 5513−5524.
(59) Vitalis, A.; Wang, X.; Pappu, R. V. Quantitative Characterization of Intrinsic Disorder in Polyglutamine: Insights from Analysis Based on Polymer Theories. *Biophys. J.* **2007**, *93*, 1923−1937.
(60) Bernado, P.; Blackledge, M. A Self-Consistent Description of the Conformational Behavior of Chemically Denatured Proteins from Nmr and Small Angle Scattering. *Biophys. J.* **2009**, *97*, 2839−2845.
(61) Marsh, J. A.; Singh, V. K.; Jia, Z.; Forman-Kay, J. D. Sensitivity of Secondary Structure Propensities to Sequence Differences between Alpha- and Gamma-Synuclein: Implications for Fibrillation. *Protein Sci.* **2006**, *15*, 2795−2804.
(62) Go, M.; Go, N. Fluctuations of an Alpha-Helix. *Biopolymers* **1976**, *15*, 1119−1127.
(63) Levy, R. M.; Karplus, M. Vibrational Approach to the Dynamics of an Alpha-Helix. *Biopolymers* **1979**, *18*, 2465−2495.
(64) Johnson, E.; Showalter, S. A.; Brüschweiler, R. A Multifaceted Approach to the Interpretation of Nmr Order Parameters: A Case Study of a Dynamic Alpha-Helix. *J. Phys. Chem. B* **2008**, *112*, 6203−6210.
(65) Das, R. K.; Pappu, R. V. Conformations of Intrinsically Disordered Proteins Are Influenced by Linear Sequence Distributions of Oppositely Charged Residues. *Proc. Natl. Acad. Sci. U. S. A.* **2013**, *110*, 13392−13397.
(66) Hendsch, Z. S.; Tidor, B. Do Salt Bridges Stabilize Proteins? A Continuum Electrostatic Analysis. *Protein Sci.* **1994**, *3*, 211−226.
(67) Meuzelaar, H.; Vreede, J.; Woutersen, S. Influence of Glu/Arg, Asp/Arg, and Glu/Lys Salt Bridges on Alpha-Helical Stability and Folding Kinetics. *Biophys. J.* **2016**, *110*, 2328−2341.

DOI: 10.1021/acs.jpcb.6b06934
J. Phys. Chem. B 2016, 120, 8960−8969

(68) Shammas, S. L.; Crabtree, M. D.; Dahal, L.; Wicky, B. I.; Clarke, J. Insights into Coupled Folding and Binding Mechanisms from Kinetic Studies. *J. Biol. Chem.* **2016**, *291*, 6689−6695.

DOI: 10.1021/acs.jpcb.6b06934
J. Phys. Chem. B 2016, 120, 8960−8969